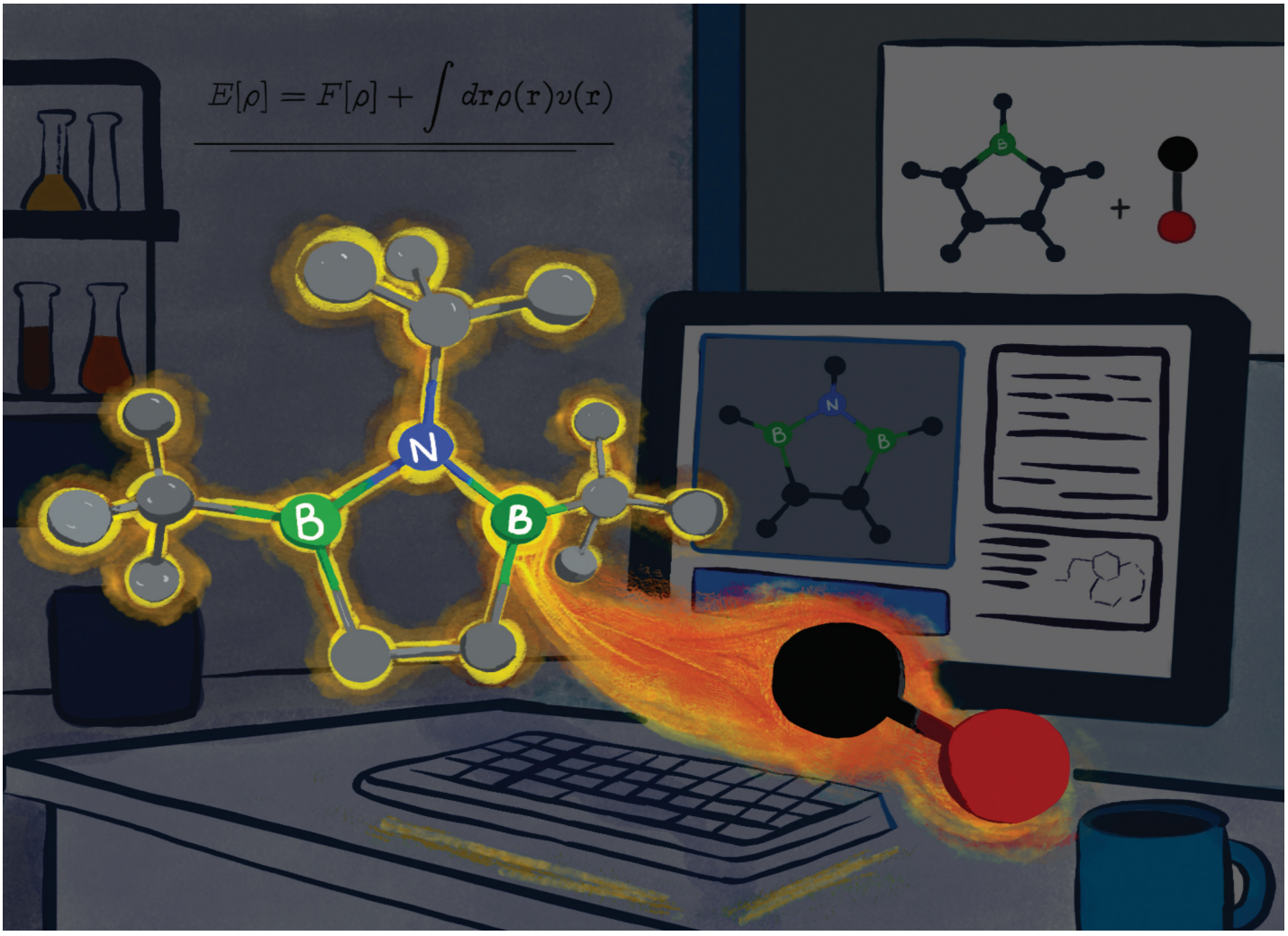

Showcasing research from Professor Jimenez-Halla's laboratory, Departamento de Química, Universidad de Guanajuato, Mexico and Professor Poater's laboratory, Institut de Química Computacional i Catàlisi, Universitat de Girona, Catalonia, Spain.

Electrophilic insertion and ring growth in 1,2,5-azadiborolidines: theoretical evidence for boron-driven expansion

DFT calculations reveal 1,2,5–azadiborolidines enable endocyclic CO insertion, viable under mild conditions, extending borole ring–expansion chemistry. Bond–length metrics and σ→π*(CO) backdonation trends predict reactivity, proposing a fourth class of CO–inserting boracycles.

Cover artwork created by Paola Rebeca González Terán.

Image reproduced by permission of Paola Rebeca González Terán from *Org. Chem. Front.*, 2025, **12**, 5146.

As featured in:

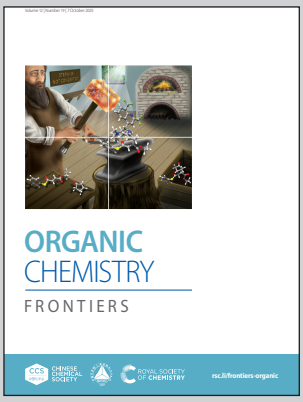

See Oscar Jimenez-Halla *et al.*, *Org. Chem. Front.*, 2025, **12**, 5146.

CCS 中国化学会 CHINESE CHEMICAL SOCIETY

SIOC 1950

ROYAL SOCIETY OF CHEMISTRY

rsc.li/frontiers-organic

ORGANIC CHEMISTRY FRONTIERS

RESEARCH ARTICLE

View Article Online
View Journal | View Issue

Cite this: *Org. Chem. Front.*, 2025, **12**, 5146

Electrophilic insertion and ring growth in 1,2,5-azadiborolidines: theoretical evidence for boron-driven expansion

Victor A. Lucas-Rosales, [a,b] Miguel A. Vázquez, [a] Gabriel Merino, *[c] Albert Poater *[b] and J. Oscar C. Jiménez-Halla *[a]

Received 26th July 2025,
Accepted 26th August 2025

DOI: 10.1039/d5qo01081k

rsc.li/frontiers-organic

This study computationally investigates the reactivity of 1,2,5-azadiborolidine derivatives toward carbon monoxide (CO), extending ring-expansion mechanisms from borole chemistry. Establishing structural and electronic analogies through isosterism, we propose that endocyclic CO insertion operates in this new class of boron heterocycles. 1,2,5-Tri-*tert*-butyl-1,2,5-azadiborolidine emerged as the optimal candidate, exhibiting a favourable three-step pathway: CO insertion, dimerization of the ring-expanded intermediate, and subsequent double [1,2]-migration. Thermochemical analysis confirms viability under mild conditions, with solvents (DCM, *n*-pentane, THF) providing similar barriers and reaction Gibbs energies. Key reactivity indicators include B–C(O) and C–O bond lengths, while correlations between kinetic barriers and $\sigma \rightarrow \pi^*$ (CO) backdonation energies provide predictive insight. This work broadens boron-based reactivity by proposing a fourth class of CO-inserting boracycles and highlights 1,2,5-azadiborolidines as versatile, metal-free frameworks for small-molecule activation.

Introduction

Ring expansion reactions remain indispensable tools in synthetic organic chemistry, offering direct access to medium- and large-sized ring systems that are often challenging to construct *via* conventional cyclization methods. These reactions provide a strategic advantage by increasing ring size without dismantling pre-existing molecular complexity, a concept widely embraced in natural product synthesis and drug design.[1] Notably, recent work by Chouraqui and co-workers emphasized the growing utility of ring expansion methodologies for synthesising structurally diverse and conformationally rich scaffolds, often with enhanced biological relevance and physicochemical properties.[2]

Ring expansions can be broadly classified into three mechanistic categories, defined by the transformation driving the ring-size increase (Chart 1).[2,3] (A) Fragmentation reactions typically involve cleavage of a small ring or leaving group, followed by rearrangement or migration to form a larger ring. These processes often proceed through carbocationic or radical intermediates and are broadly applied in skeletal editing. (B) Pericyclic reactions (*e.g.*, electrocyclic ring openings, sigmatropic rearrangements, and cycloadditions) proceed *via* concerted mechanisms governed by orbital symmetry and have been central in synthesising polycyclic and strained architectures. (C) Insertion reactions, the focus of this study, entail the formal incorporation of an external atom or functional group into a cyclic framework. These transformations frequently proceed under mild conditions with high regiochemical and stereochemical control, rendering them particularly attractive for constructing complex, functionalized ring systems.

Among the elements used in insertion strategies, boron stands out due to its unique electron-deficient character,

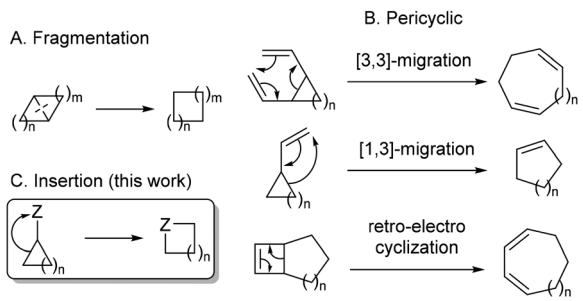

Chart 1 Classification of ring expansion reactions.

[a]*Departamento de Química, División de Ciencias Naturales y Exactas, Universidad de Guanajuato, Noria Alta S/N 36050, Guanajuato, Guanajuato, Mexico. E-mail: jjimenez@ugto.mx*
[b]*Institut de Química Computacional i Catàlisi, Departament de Química, Universitat de Girona, C/Mª Aurèlia Capmany 69, 17003 Girona, Catalonia, Spain. E-mail: albert.poater@udg.edu*
[c]*Departamento de Física Aplicada, CINVESTAV, Unidad Mérida, Km 6 Antigua Carretera a Progreso. Apdo. Postal 73, Cordemex, 97310 Mérida, Yucatán, Mexico. E-mail: gmerino@cinvestav.mx*

which enables distinctive bonding modes and electrophilic reactivity not typically observed in classic organic systems.[4–9] The incorporation of boron atoms into molecular frameworks facilitates the development of advanced materials with potential applications across diverse fields, including energy storage,[10–17] optoelectronics,[17–21] drug design,[22–24] and small molecule activation.[9,17,25–27]

Within this landscape, ring expansion reactions in boracycles constitute a powerful subclass, enabling access to structurally diverse and electronically tunable organoboron architectures.[28–31] However, there is a reduced number of heterocycles containing trivalent boron atoms that can activate carbon monoxide (CO) *via* a coordination–insertion mechanism (Chart 2). For instance, early work by Paetzold and Boese showed that a *tert*-butyl-substituted azadiboriridine (NB_2R_3) undergoes 1,1-insertion with carbon monoxide (CO), followed by dimerization and a [1,2]-migration to afford a six-membered diboroxan heterocycle.[32] Siebert subsequently provided mechanistic insights into a related boron-mediated ring expansion *via* CO insertion, dimerization, and rearrangement.[33] More recently, Piers and co-workers expanded the synthetic utility of such transformations by developing transition-metal-free ring expansion of boroles, yielding larger boracycles with improved stability and applications in materials chemistry.[34]

Given that boroles and 1,2,5-azadiborolidines share analogous structural and electronic features, they can be viewed as isosteres. We thus hypothesized that 1,2,5-azadiborolidines could undergo similar reactivity toward CO insertion, ring expansion, or dimerization. Frontier molecular orbitals (particularly the LUMO centred on boron) could likewise behave analogously in electrophilic or π-system reactions, as shown for boroles. However, early experimental studies revealed different reactivity for azadiborolidines due to adjacent electron-deficient boron centres and a lone pair-bearing nitrogen.[35–39]

Recent work highlights azadiborolidines as tunable reactivity platforms: Brown[40] and Hu and Cui[41] showed strategic functionalization to modulate their reactivity with small molecules like CO, enabling ring-expanded heterocycles and synthetically relevant boron–heteroatom linkages. These transformations underscore the flexibility of the B–N–B core as both a structural and reactive unit.

Beyond small-molecule activation, azadiborolidines and related BN-heterocycles exhibit promising electronic and optical properties. Studies by Wu, Zeng and co-workers[42] and Narita and Müllen[43] explain how N–B incorporation into π-conjugated systems influences aromaticity, stability, and electronic delocalization, highlighting their potential in organic electronic and optoelectronic applications. The polar N–B bond facilitates fine-tuning of HOMO–LUMO gaps while maintaining the planarity and delocalization essential for conjugated systems.

The present study investigates the hypothesis that borole and 1,2,5-azadiborolidine rings exhibit similar reactivity concerning the CO-induced ring expansion reaction, and subsequently, extending this to dimerization processes for the formation of highly complex fused boracycles. Herein, we employ density functional theory (DFT) to assess the viability of these reactions in 1,2,5-azadiborolidines, specifically addressing substituent effects. The main objective of this work is to predict the CO insertion reaction in any of the previously synthesised 1,2,5-azadiborolidine derivatives, for which no reaction with CO has been reported to date. Furthermore, this research aims to identify reactivity descriptors capable of explaining such a transformation, thereby broadening the theoretical insights into this class of reactions in boracycle chemistry.

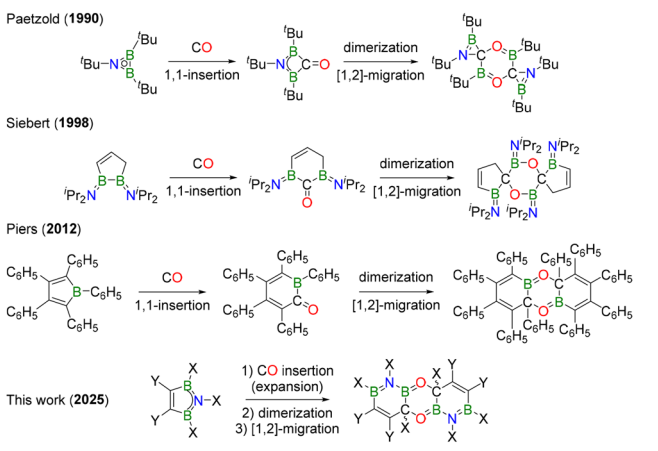

Chart 2 CO insertion-induced ring expansion reactions in boracycles.

Computational methods

DFT calculations were performed using Gaussian 09.[44] The long-range hybrid functional ωB97X-D was employed with the Ahlrichs split-valence def2-SVP basis set for all atoms.[45,46] Geometry optimisations were conducted in the gas phase without constraints. Initial coordinates were extracted from crystallographic data where available. Harmonic frequency calculations characterised stationary points. Thermal corrections to Gibbs energies were obtained under the ideal gas approximation at 298.15 K and 1 atm. Electronic energies were refined *via* single-point calculations using the def2-TZVPP basis set.[46] Solvent effects were incorporated *via* the polarizable continuum model (PCM) with SMD parameters, using dichloromethane (DCM), *n*-pentane, and tetrahydrofuran (THF) as representative solvents common in the synthesis of such molecules.[47] Gibbs energies thus correspond to the ωB97X-D/def2-TZVPP//ωB97X-D/def2-SVP level. This approach provides an effective balance between accuracy and computational cost.[48,49]

The global electrophilicity index (ω),[50] defined as $\omega = \mu^2/2\eta$, where μ is the chemical potential and η is the hardness, serves as a reactivity descriptor. Within the ground-state parabolic model, μ and η were approximated using the vertical ionization potential (I) and electron affinity (A), yielding $\omega = (I + A)^2/8(I - A)$. Applying Pearson's principle[51] and using Koopmans' theorem,[52] I and A can be approximated as the negative values

of the HOMO and LUMO energies, ε_{HOMO} and ε_{LUMO}, respectively. This leads to the working equation: $\omega = (\varepsilon_{HOMO} + \varepsilon_{LUMO})^2/8(\varepsilon_{LUMO} - \varepsilon_{HOMO})$. Although strictly valid for Hartree–Fock theory, the utility of this approximation in conceptual DFT is well established.[53–56] Frontier orbital energies were computed at the gas-phase single-point refinement level.

Geometrical descriptors, specifically the molecular planarity parameter (MPP) and the span of deviation from planarity (SDP),[57] were calculated for the starting heterocycles. Additionally, steric hindrance was evaluated by calculating buried volumes (% V_{Bur}) and generating steric maps using SambVca 2.1.[58–61]

Further wavefunction analysis used NBO and Multiwfn software.[62,63] The Mayer[64] and Wiberg[65] bond indices (MBI and WBI) were estimated at the ωB97X-D/def2-TZVPP//ωB97X-D/def2-SVP level. The WBI values were calculated in the Löwdin orthogonalized basis.[66] The multicentre index (MCI) was computed within the natural atomic orbital (NAO) framework,[67–70] while σ → π*(CO) backdonation energies were quantified *via* second-order perturbation theory analysis of the Fock matrix in the NBO basis. Because of the delocalized nature of these interactions, diffusion functions were essential; analyses were therefore performed at the ωB97X-D/def2-TZVPPD level on optimised gas-phase geometries.[71]

Results and discussion

We initially explored the ring expansion reactivity of borole derivatives with CO, focusing on the parent borole (**1**), pentaphenylborole (**2**), and perfluoropentaphenylborole (**3**). Compounds **2** and **3** were previously studied experimentally by Piers and co-workers,[34] providing a benchmark to assess electronic and steric effects on the thermodynamics and kinetics of CO-mediated ring expansion. These boroles were later compared with 1,2,5-azadiborolidines to quantify energetic requirements for analogous pathways.

The proposed mechanism comprises two key steps (Scheme 1). First, the formation of Lewis adducts through CO coordination to boron, followed by 1,1-insertion of CO *via endocyclic* (ring B–C bond) or *exocyclic* (exterior B–C bond) pathways.

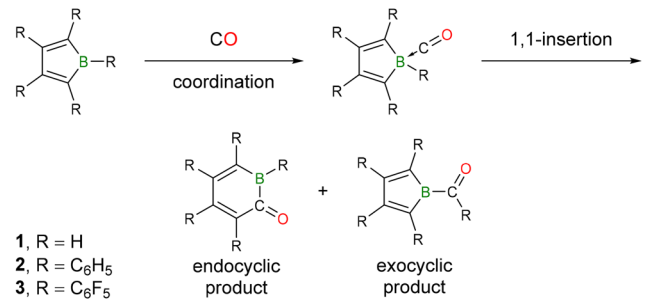

Scheme 1 A plausible reaction mechanism for the CO insertion into boroles (R = –H, $-C_6H_5$, $-C_6F_5$). The endocyclic product refers to the ring expansion reaction.

As shown in Fig. 1, CO coordination is spontaneous for all the boroles ($\Delta G_{R\rightarrow I\text{-}1}$) with low energy barriers ($\Delta G^{\ddagger}_{R\rightarrow TS-1}$), indicating an equilibrium clearly shifted towards the adduct **I-1**. Furthermore, the energetic analysis indicates kinetically reversible CO coordination before ring expansion for **2** ($\Delta G^{\ddagger}_{I-1\rightarrow TS-1}$ = 10.9; $\Delta G^{\ddagger}_{I-1\rightarrow TS-2}$ = 17.9; $\Delta G_{I\text{-}1\rightarrow P\text{-}1}$ = 16.1 kcal mol^{-1}) and **3** ($\Delta G^{\ddagger}_{I-1\rightarrow TS-1}$ = 11.4; $\Delta G^{\ddagger}_{I-1\rightarrow TS-2}$ = 30.1; $\Delta G_{I\text{-}1\rightarrow P\text{-}1}$ = 16.3 kcal mol^{-1}), aligning with experimental findings.[34] Note that the endocyclic insertion is kinetically feasible at room temperature for **1** and **2**, although only **1** affords a thermodynamically stable product ($\Delta G_{R\rightarrow P\text{-}1}$ = −2.9 kcal mol^{-1}).

The substituent effects in boroles **1–3** are significant in the thermochemistry of the ring expansion reaction. Firstly, a reduction in the exergonic character of the CO coordination step is observed, accompanied by an increase in the corresponding energy barriers. This destabilization occurs when phenyl (**2**), a modest π-donor group, and perfluorophenyl (**3**), a moderately inductive electron-withdrawing and weak π-donor group, are considered as substituents. Sterically, **1** is least hindered, whereas **2** and **3** present comparable aryl bulk. Consequently, the general thermodynamic and kinetic destabilization of the coordination step for **2** (R = $-C_6H_5$) and **3** (R = $-C_6F_5$) can be attributed to the increased volume of the substituents surrounding these rings compared to **1** (R = –H). Furthermore, Lewis adduct formation is favoured both kinetically and thermodynamically for **3** over **2**. This outcome can be rationalized by examining the electronic structure of boroles: the perfluoro derivative (**3**) bears substituents that behave more as electron-withdrawing groups. This enhances the electrophilicity of the ring compared to **2**. Therefore, the interaction with CO (a σ-donor/π-acceptor ligand) is expected to be more effective when utilising **3**, a greater electrophile, than when using **2**. The last reasoning is also supported by ω values: 1.519 (**1**), 1.446 (**2**), and 2.479 (**3**) eV.

A similar counterproductive effect is recognised for the thermodynamics of the endocyclic insertion step ($\Delta G_{I\text{-}1\rightarrow P\text{-}1}$), which can be explained by the same previous arguments: the thermodynamics is generally destabilized for **2** and **3**, in comparison with **1**, due to the presence of bulkier groups; the electronics of the substituents differentiate the energetic require-

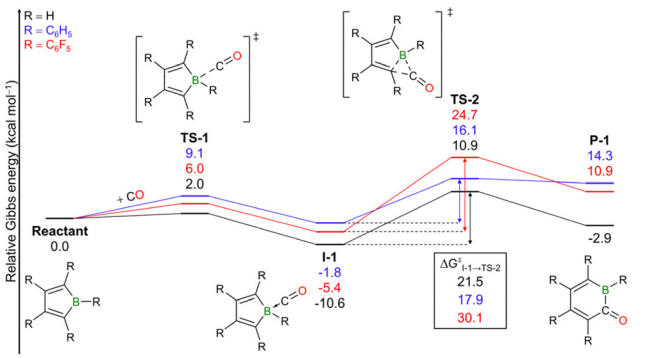

Fig. 1 Relative Gibbs energy profiles (kcal mol^{-1}) in the gas phase for the ring expansion reaction of selected borole derivatives with CO.

ments for the phenyl (**2**) or perfluorophenyl (**3**) derivatives. Nevertheless, the kinetics of the endocyclic 1,1-insertion step ($\Delta G^{\ddagger}_{I-1\rightarrow TS-2}$) depends primarily on electronics rather than steric effects. Notably, borole **2** has a smaller barrier height despite having bulkier substituents than **1**; sterically, **TS-2** of **2** and **3** have similar environments (Fig. S1), yet there is a 12.2 kcal mol^{-1} difference in energy barriers ($\Delta\Delta G^{\ddagger}_{I-1\rightarrow TS-2}$). Also, the trend of the ω values **2** < **1** < **3** correlates with the insertion barrier energies ($\Delta G^{\ddagger}_{I-1\rightarrow TS-2}$), suggesting that higher ω stabilizes the pre-insertion complex but increases substrate distortion at **TS-2**, thereby elevating the barrier in **3** compared with **2**. Interestingly, the C2–B and B–C lengths in Fig. S1 follow the same trend. Exocyclic pathways exhibit higher barriers and endergonic profiles (Fig. S2).

These computational findings align with experimental results reported by Piers and coworkers.[34] Compound **2** forms the Lewis adduct **I-1** in CH_2Cl_2 at −78 °C. Upon warming to −10 °C, NMR spectroscopy reveals primarily the dimerized ring-expansion product rather than the monomer (Chart 3a). The absence of a monomer is consistent with thermochemical data identifying the ring-expansion intermediate as unstable ($\Delta G_{R\rightarrow P\text{-}1}$ = 14.3 kcal mol^{-1}). For **3**, the Lewis adduct is well characterised by X-ray crystallography (CCDC 863188),[34] yet no insertion product is formed even at high temperatures (Chart 3b), consistent with the high energy barrier for the endocyclic CO insertion ($\Delta G^{\ddagger}_{I-1\rightarrow TS-2}$ = 30.1 kcal mol^{-1}). In contrast, while experimental data for **1** remain unavailable, our results suggest that its ring expansion, a pivotal step before dimerization, is reversible and feasible under appropriate thermal control. Moreover, these results show excellent agreement with the energy profiles of Lin, including dimerization pathways and solvent effects.[72]

Given the shared central heterocyclic framework of boroles **1–3**, we focus on **1** for a detailed discussion. Note that 1,2,5-azadiborolidine (**4**) exhibits structural similarity to borole, theoretically derived by replacing a C=C double bond with an isoelectronic N=B double bond adjacent to the ring boron atom. This substitution, termed heteroatom doping, is a well-established strategy for tuning electronic properties.[73–78]

As shown in Fig. 2, both **1** and **4** adopt C_{2v} symmetry and the $^1A_1$ singlet ground state. Their adiabatic singlet–triplet energy gaps, ΔE_{ST} = 20.9 (**1**) and 51.0 (**4**) kcal mol^{-1}, confirm the singlet as the ground state for both cases. As 4π-electron systems, they display antiaromatic character, as evidenced by their low multicentre indices (MCI).[79–81] Notably, **4** shows greater electronic delocalization across the ring, reflected in its higher MCI value relative to **1**. This enhanced delocalization in **4** correlates with a lower global electrophilicity index, indicating a reduced electrophilic character compared to **1**. MCI analysis of the lowest-lying triplet states (C_{2v}, $^3B_2$) reveals increased delocalization in both molecules, in agreement with Baird's rule, which predicts aromaticity in triplet-state 4π-systems.[82–84] Accordingly, while **1** is more antiaromatic in the singlet state, it becomes more aromatic than **4** in the triplet state. This shift in aromatic character explains the significantly lower ΔE_{ST} observed in **1**, as aromatic stabilization in the triplet state contributes to its energetic favourability.[85,86]

Geometric analysis reveals similar B–C (1.587–1.592 Å) and C=C (1.343–1.349 Å) bond lengths in compounds **1** and **4**. In 1,2,5-azadiborolidine, the N–B bonds are fully equalized, with bond lengths (1.432 Å) closely matching the borazine values from X-ray crystallography (1.429 Å (ref. 87) and 1.427–1.429 Å (ref. 88)). This supports a borazine-like bonding structure in the B–N–B fragment, consistent with Yáñez's computational studies,[89] indicating nitrogen lone-pair delocalization over the B–N–B moiety as the optimal Lewis representation (Fig. 2).

The MBI values indicate that the C=C bond is stronger at **1**, whereas the B–C bond exhibits greater stability at **4**. Furthermore, a comparison of the B–C and N–B bond indices in **4** reveals that the latter is of higher order, in agreement with preceding discussions.

Frontier molecular orbital analysis (Fig. S3) reveals a key distinction: while the HOMOs and LUMOs of **1** and **4** share identical symmetry and shape and comparable energies, their ordering is reversed, **1**-HOMO resembles **4**-LUMO, and *vice versa*. Consequently, these systems are not isolobal; however, they constitute isosteres under current IUPAC definitions.[90,91]

Despite lacking isolobal equivalence, their isosteric properties suggest analogous reactivity. Therefore, we examined

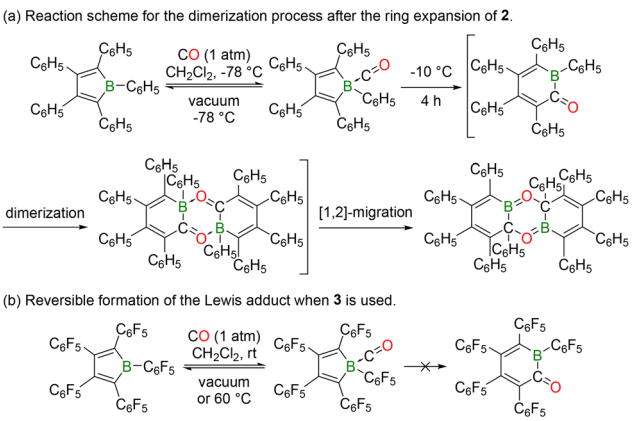

Chart 3 Experimental evidence for the CO insertion reactions of **2** and **3**.

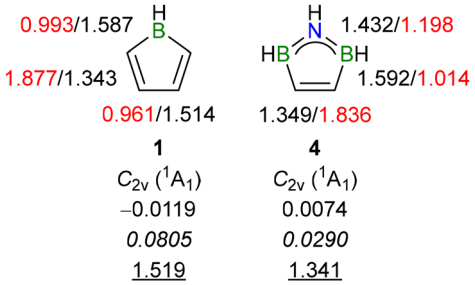

Fig. 2 Comparison of the structural, symmetric, reactivity, and electronic features between borole (**1**) and 1,2,5-azadiborolidine (**4**). Bond lengths are expressed in Å, singlet- and triplet-state (italics) MCI values in electrons, and global electrophilicity (underline) in eV. MBI values in red.

the two-step CO reaction mechanism (coordination followed by 1,1-insertion) for 1,2,5-azadiborolidine derivatives. Given asymmetric endocyclic bonds adjacent to boron (N–B *vs.* B–C), we also evaluated insertion at the N–B bond—termed NB-endocyclic insertion (Scheme 2).

We used previously synthesised azadiborolidines as starting materials (Chart 4). Haubold and co-workers reported the first synthesis in 1980 (1,2,3,4,5-pentamethyl derivative **5**),[35] followed months later by Siebert's 3,4-diethyl-1,2,5-trimethyl-1,2,5-azadiborolidine (**6**).[36] Köster and co-workers advanced the field in 1994 by introducing trimethylsilyl substituents (*e.g.*, **7**).[38] Paetzold's pioneering work on azadiboriridine reactivity subsequently enabled derivatives 1,2,5-tri-*tert*-butyl-1,2,5-azadiborolidine (**8**) and 1,2,5-tri-*tert*-butyl-3,4-dimethyl-1,2,5-azadiborolidine (**9**).[37,39] These compounds have only been characterised by NMR and MS to date.

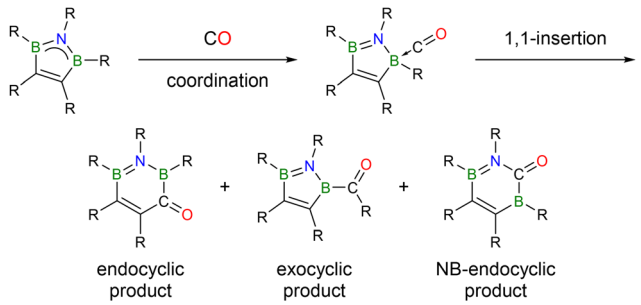

Scheme 2 A plausible reaction mechanism between 1,2,5-azadiborolidine derivatives and CO. The endocyclic products refer to the ring expansion reaction.

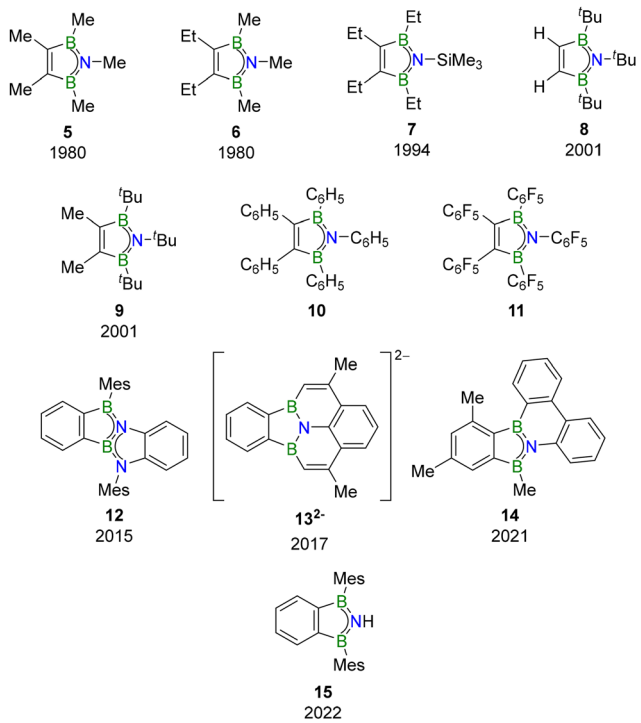

Chart 4 Overview of 1,2,5-azadiborolidine derivatives considered in this work.

Hypothetical pentaphenyl (**10**) and fluorinated pentaphenyl (**11**) analogues, designed by similarity to boroles **2** and **3**, were also computationally examined. Conversely, compounds **12–15** have been structurally authenticated: **12** by Müllen (CCDC 1412367);[43] dianion $\mathbf{13}^{2-}$ by Zeng (CCDC 1555140);[42] **14** by Cui (CCDC 2045630),[41] and **15** by Lindley (CCDC 2122486).[40] Beyond these, only the 1,2,5-azadiborolidines by Piers, in 2004, and Li, in 2020, have been reported.[92,93]

Given the experimental confirmation that borole **2** undergoes ring expansion, while **3** does not, we then evaluated CO insertion feasibility in 1,2,5-azadiborolidines using previously derived kinetic and thermodynamic profiles.

In contrast to boroles **2** and **3**, the CO coordination for 1,2,5-azadiborolidine derivatives is endergonic, exhibiting higher energy barriers in all cases (Table 1). The rate-determining step remains ring expansion (**R** → **TS-2**), yet the reaction Gibbs energy ($\Delta G_{R\rightarrow P\text{-}1}$) is consistently lower than that for borole **2** ($\Delta G_{R\rightarrow P\text{-}1}$ = 14.3 kcal mol^{-1}). This indicates thermodynamic favourability upon replacing the borole with a 1,2,5-azadiborolidine unit. For instance, compounds **4**, **12**, and **13** show $\Delta G_{R\rightarrow P\text{-}1}$ values near equilibrium (0.1, −0.4, and 1.3 kcal mol^{-1}, respectively). Kinetically, however, endocyclic CO insertion faces higher barriers than **2**. In particular, heterocycles **8** and **9** show barriers ($\Delta G^{\ddagger}_{R\rightarrow TS-2}$ = 23.9 and 26.8 kcal mol^{-1}, respectively) exceeding **2** but below **3**, suggesting ring expansion at increased temperatures or extended reaction times; a comparison of relevant **TS-2** structural parameters for **1–3** and **8** is presented in Fig. S1. In contrast, **4** and **7** exhibit barriers

Table 1 Relative Gibbs energy values (kcal mol^{-1}) in the gas phase for the ring expansion reaction between different 1,2,5-azadiborolidine derivatives and CO[a]

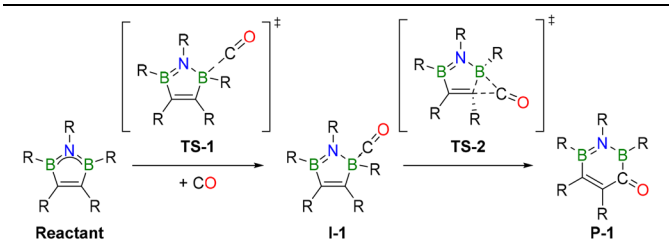

Entry	Reactant	TS-1	I-1	TS-2	P-1
1	**8**	15.2	11.2	23.9	11.4
2	**9**	17.4	14.2	26.8	11.0
3	**4**	11.8	8.2	30.0	0.1
4	**7**	15.1	12.3	30.5	7.1
5	**10**	15.9	13.7	31.9	13.9
6	**5**	16.4	15.9	33.8	4.7
7	**6**	16.3	15.7	34.9	5.2
8	**15**	22.5	21.6	37.5	4.8
9	**12**	22.0	21.4	37.8	−0.4
10	**14**	14.8	14.2	39.2	6.6
11	**11**	12.4	10.1	41.1	12.3
12	**13**	22.4	22.1	45.9	1.3

[a] Entries follow a natural order with respect to **TS-2**.

near 30.0 kcal mol^{-1}, rendering ring expansion unlikely under standard conditions. The remaining derivatives (entries 5–12) display even higher barriers ($\Delta G^{\ddagger}_{R\rightarrow TS-2}$ > 30.1 kcal mol^{-1}), substantially diminishing the prospect of CO insertion under experimental conditions.

Exocyclic insertion is noncompetitive for **5–7**, **11–12**, and **15**, yet it yields the kinetic product for **4** and **13–14** (Table S1). Conversely, it affords the thermodynamic product for **8–10**. NB-endocyclic insertion, tested representatively for **4**, **5**, **8**, and **10**, proved noncompetitive (Table S2), likely due to cleavage of the delocalized B–N–B bond during insertion, which compromises ring stability. This underscores the greater strength of the N–B bond relative to the inherently labile B–C bond in boroles,[29,94] as suggested by bond lengths, MBI and WBI reported in Tables S3–S8.

Given the presence of an electron-rich nitrogen and an electron-deficient boron in 1,2,5-azadiborolidines, dimerization was considered plausible and then examined computationally. Calculations for all derivatives (Fig. S4), except **12–15** (for which single-crystal X-ray data show monomeric structures incompatible with the dimeric motif evaluated), reveal favourable dimerization only for **4**. For **5**, the reaction Gibbs energy (5.9 kcal mol^{-1}) and barrier (17.1 kcal mol^{-1}) align with the experimental detection of only a trace dimer by NMR.[35] Increasing the substituent size elevates both the energy and barrier, confirming high steric sensitivity.

Across the examined 1,2,5-azadiborolidines, the optimised geometries reveal an average N–B bond length of 1.446 Å (σ = 0.009 Å). Despite the lost bond equalization in the B–N–B moiety, the N–B lengths remain borazine-like, supporting similar electronic character. This observation is replicated when analysing MBI and WBI data (Tables S4 and S5). Notice that most rings are planar, except **8**, **9**, and **14**, as revealed by large MPP and SDP values (Table S3); their out-of-plane distortions relieve steric strain from bulky substituents (*e.g.*, *tert*-butyl groups in **8** and **9**).

For the adduct **I-1**, the average B–C(O) and C–O bond lengths are 1.622 Å (σ = 0.043 Å) and 1.129 Å (σ = 0.003 Å), respectively (Table S6). The MBI specifies a bond order of 0.575–0.877 for B–C(O), and 2.301–2.427 for the C–O bond (Table S7), whereas the WBI estimates slightly stronger bonds (Table S8): 0.910–1.178 and 3.056–3.130 values, respectively. The initial delocalization along the B–N–B fragment is lost when forming the Lewis adduct, as supported by both MBI and WBI values (Tables S4, S5, S7 and S8). Moreover, as illustrated in the Lewis structures in Table S7, MBI examination suggests a dative bond between the CO fragment and the boracycle, *i.e.*, a B ← C(O) bond, while highlighting a general decrease in the C–O bond order, thus indicating a likely donor → π*(CO) backdonation.

A systematic analysis quantified key thermochemical correlations across azadiborolidine and borole derivatives (Fig. 3). The strongest correlation (R^2 = 0.9544) was found between the energy barrier for CO coordination ($\Delta G^{\ddagger}_{R\rightarrow TS-1}$) and its reaction Gibbs energy ($\Delta G_{R\rightarrow I\text{-}1}$). A secondary correlation (R^2 = 0.8487) was obtained between the ring expansion barrier and B–C(O)

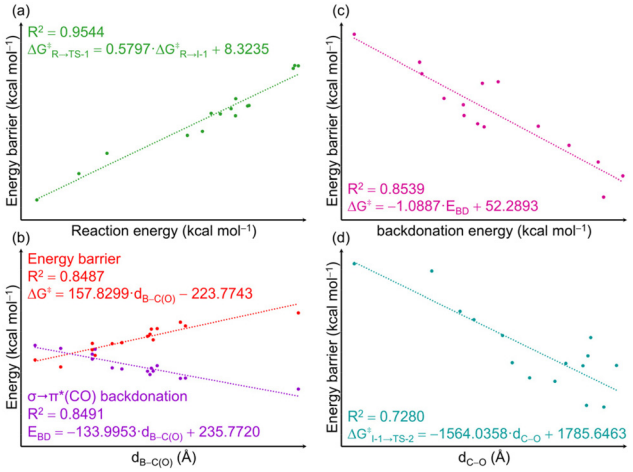

Fig. 3 Analysis of linear correlations from gas-phase thermochemistry data for the endocyclic CO insertion among compounds **1–15**. (a) Energy barrier and reaction energy of the CO coordination step. (b) Total energy barrier and σ → π*(CO) backdonation energy related to the B–C(O) bond length. (c) Total energy barrier and backdonation energy. (d) Energy barrier of the second reaction step and the C–O bond length. The σ → π*(CO) backdonation energies and the B–C(O) and C–O bond lengths were calculated for the adduct **I-1**.

bond length. Second-order perturbation analysis of **I-1** quantified stabilization energies from donor–acceptor NBO interactions, specifically concerning σ → π*(CO) backdonation. The total energetic stabilization performed by the two endocyclic σ-NBOs related to the boron centre reveals a significant correlation with the B–C(O) bond length (R^2 = 0.8491) and with the total barrier (R^2 = 0.8539). Notably, using average backdonation energies (*cf.* Piers *et al.*[34]) substantially reduced the correlation coefficients (Fig. S5). We thus recommend employing *total* (not average) σ → π*(CO) backdonation energies for future studies of such adducts. Remarkably, a moderate correlation coefficient (R^2 = 0.8291) was calculated between the backdonation energy and WBI for the C–O bond. Also, when considering the MBI of the B–C(O) bond, a significant coefficient (R^2 = 0.8343) emerged in relation to the total energy barrier.

A reasonable correlation was found between the CO insertion barrier ($\Delta G^{\ddagger}_{I-1\rightarrow TS-2}$) and the C–O bond length (R^2 = 0.7280). However, no meaningful correlations emerged between the C–O bond length and either the B–C(O) bond length or backdonation energy. A weak correlation was also noted between ω and the ring expansion barrier (R^2 = 0.6950, Fig. S5c). This trend contradicts Parr's principle, which states that higher ω values correspond to greater electron-accepting ability and, therefore, higher reactivity.[50] Piers previously identified this apparent *paradox*,[34] suggesting that the dependency of σ → π*(CO) backdonation on the initial electrophilicity of the ring may explain it. However, our computations indicated that the correlation between ω and backdonation is negligible (Fig. S5d), and is weaker than those shown in Fig. 3. Complete electrophilicity and σ → π*(CO) backdonation data are provided in Tables S3 and S9–S10, respectively.

Additional insights were obtained from the analysis of the steric environment in **I-1** (Fig. S6). First, steric hindrance remains largely unchanged upon replacing the borole ring with a 1,2,5-azadiborolidine core. Second, $\%V_{Bur}$ is more sensitive to the substituent size at positions 1, 2, and 5 than at positions 3 and 4 of the heterocycle. Third, substitution of hydrogen with fluorine significantly increases $\%V_{Bur}$. Although fluorination is often employed to enhance ring electrophilicity, it may also compromise the steric environment of the Lewis adduct. Nonetheless, neither the planarity of the starting ring (*e.g.*, MPP and SDP) nor the steric hindrance (*e.g.*, $\%V_{Bur}$) in **I-1** was found to be a significant predictor of the thermochemistry of the CO-induced ring-expansion reaction.

Given that the experimental final product of borole **2** is its dimer rather than the ring-expanded monomer, we explored the dimerization energy profile for 1,2,5-azadiborolidine derivatives. Focusing on **8**, the most promising candidate based on ring expansion energetics, we calculated the extended profile (Fig. 4). Following CO-induced ring expansion of **8** (**R** → **P-1**), viable dimerization (**P-1** → **I-2**) occurs, succeeded by double [1,2]-migration of boron substituents (**I-2** → **P-2**). Here, **P-1** is a kinetically trapped, low-temperature isolable intermediate, whereas **P-2** is the thermodynamically preferred product formed upon subsequent conversion of **P-1**. Dimerization proceeds concertedly through **TS-3**, aligning with the product hierarchy of borole **2** [34] but differing mechanistically: **8** dimerizes concertedly, whereas **2** follows a stepwise pathway.[72] The transformation is highly exergonic ($\Delta G_{R\rightarrow P\text{-}2}$ = −62.2 kcal mol^{-1}) with a thermally accessible total barrier ($\Delta G_{R\rightarrow TS\text{-}3}$ = 25.3 kcal mol^{-1}).

To better approximate experimental conditions (where 1,2,5-azadiborolidine syntheses typically employ DCM, *n*-pentane, or THF), we analysed solvent effects. For compound **8**, the energetic impact is most pronounced during 1,1-endocyclic CO insertion (**R** → **P-1**). The barrier $\Delta G^{\ddagger}_{R\rightarrow TS-2}$ decreases from 23.9 kcal mol^{-1} (gas-phase) to 19.0 kcal mol^{-1} in THF, while $\Delta G_{R\rightarrow P\text{-}1}$ drops from 11.4 kcal mol^{-1} to 4.8 kcal mol^{-1} in DCM. For the full profile, dimerization of the expanded ring **P-1** remains rate-determining. The barrier $\Delta G^{\ddagger}_{R\rightarrow TS-3}$ is consistent across solvent environments: 25.9 (THF), 25.4 (DCM), 25.3 (gas), and 25.3 kcal mol^{-1} (*n*-pentane). Although solvents slightly destabilize the overall reaction ($\Delta G_{R\rightarrow P\text{-}2}$ = −60.6 to −62.2 kcal mol^{-1}), deviations are minimal. Therefore, across THF, DCM, and *n*-pentane, the computed solvent effects are modest: the differences in $\Delta G^{\ddagger}$ are ≤0.5 kcal mol^{-1} at 298 K. THF and DCM afford essentially comparable kinetic and thermodynamic profiles, while *n*-pentane shows a slightly lower barrier; however, the magnitude of these differences lies within the uncertainty of the method. We therefore conclude that all three solvents provide functionally similar outcomes under our conditions.

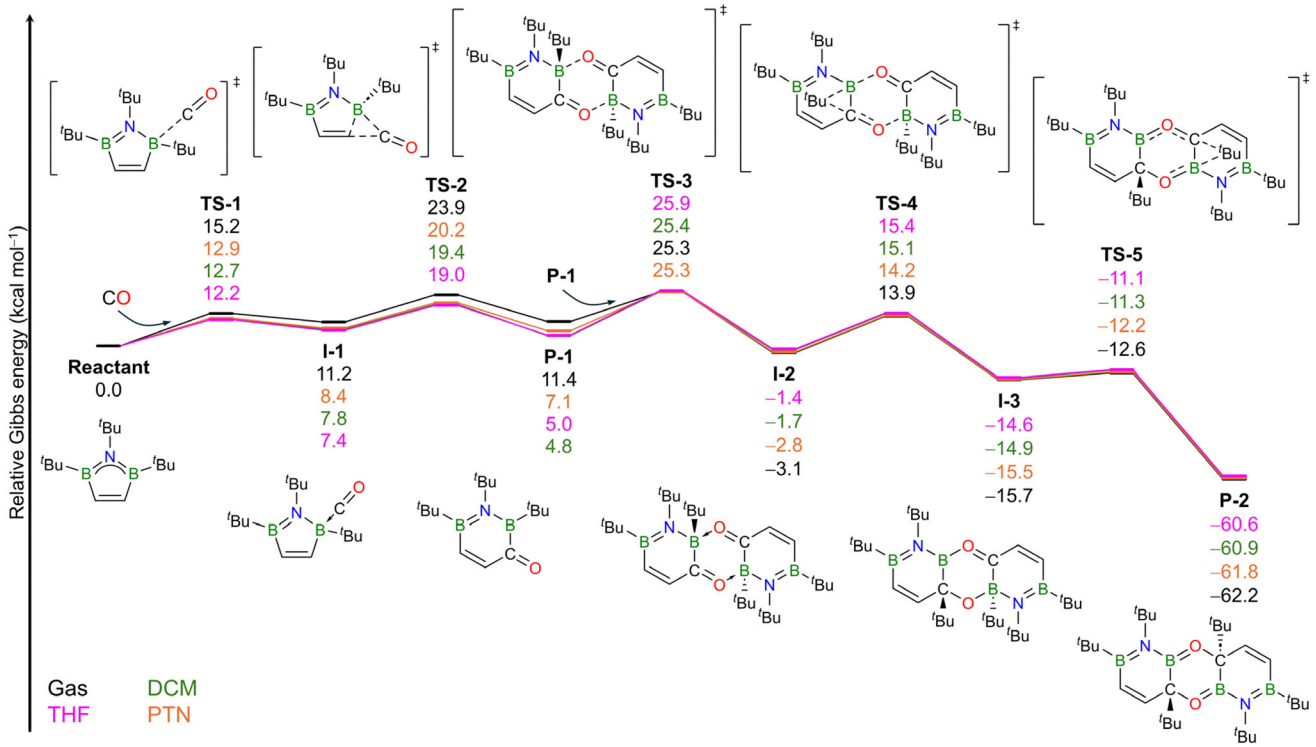

Fig. 4 Relative Gibbs energy profile for the ring expansion of **8** with CO, followed by a dimerization process and a subsequent double [1,2]-migration of the central *tert*-butyl substituents. Energy values (kcal mol^{-1}) were calculated in the gas phase and three solvents: dichloromethane (DCM), *n*-pentane, and tetrahydrofuran (THF).

Conclusions

We performed a computational study to elucidate the mechanism of endocyclic CO insertion into borole rings. Establishing a structural analogy *via* isosterism between boroles and 1,2,5-azadiborolidines enabled the transposition of CO ring expansion to this unexplored boron heterocycle. For the optimal candidate (**8**), the pathway comprises: (1) CO-induced ring expansion, (2) dimerization, and (3) double [1,2]-migration, mirroring borole mechanisms. These results confirm that **8** exhibits comparable CO reactivity alongside structural similarity to boroles. Computations predicted viable CO insertion[95] for **8**, yielding polycyclic **P-2**. Within the accuracy of our calculations, no single solvent is uniquely optimal; THF, DCM, and *n*-pentane provide similar barriers and reaction Gibbs energies.

Mechanistically, the B–C(O) and C–O bond lengths in Lewis adducts correlate with ring expansion kinetics. A significant correlation between $\sigma \rightarrow \pi^*(CO)$ backdonation energies and reaction barriers highlights its utility as a predictive descriptor for boron systems. We encourage experimental validation to establish 1,2,5-azadiborolidine as the fourth trivalent-boron-containing heterocycle undergoing CO coordination–insertion, highlighting the metal-mimetic behaviour of boron and enabling design of novel functional materials.

Author contributions

Victor A. Lucas-Rosales: investigation, validation, formal analysis, writing – original draft. Miguel A. Vázquez: investigation, writing – review. Gabriel Merino: investigation, writing – review. Albert Poater: supervision, formal analysis, computational resources, funding acquisition. J. Oscar C. Jiménez-Halla: conceptualization, supervision, formal analysis, funding acquisition.

Conflicts of interest

There are no conflicts to declare.

Data availability

The data supporting this article have been included as part of the SI: Cartesian coordinates of optimised geometries and electronic structure analyses. See DOI: **https://doi.org/10.1039/d5qo01081k**.

Acknowledgements

V. A. L.-R. thanks SECIHTI for his M.Sc. student scholarship (#1312084). J. O. C. J.-H. acknowledges Laboratorio Nacional de Cómputo de Alto Desempeño (PIPILA) and Universidad de Guanajuato (DCNE). A. P. is a Serra Húnter Fellow and thanks the Spanish MINECO for project PID2021-127423NB-I00, and the Generalitat de Catalunya for project 2021SGR623. The authors acknowledge the computing time supported by Conacyt (Grant CB-2015-252356), and additional resources provided by BSC supercomputing facilities.

References

1 E. J. Kantorowski and M. J. Kurth, Expansion to Seven-Membered Rings, *Tetrahedron*, 2000, **56**, 4317–4353.
2 B. Biletskyi, P. Colonna, K. Masson, J.-L. Parrain, L. Commeiras and G. Chouraqui, Small rings in the bigger picture: ring expansion of three- and four-membered rings to access larger all-carbon cyclic systems, *Chem. Soc. Rev.*, 2021, **50**, 7513–7538.
3 J. R. Donald and W. P. Unsworth, Ring-Expansion Reactions in the Synthesis of Macrocycles and Medium-Sized Rings, *Chem. – Eur. J.*, 2017, **23**, 8780–8799.
4 Y. Shoji, N. Tanaka, K. Mikami, M. Uchiyama and T. Fukushima, A two-coordinate boron cation featuring C–B^+–C bonding, *Nat. Chem.*, 2014, **6**, 498–503.
5 H. Braunschweig, T. Dellermann, W. C. Ewing, T. Kramer, C. Schneider and S. Ullrich, Reductive Insertion of Elemental Chalcogens into Boron–Boron Multiple Bonds, *Angew. Chem., Int. Ed.*, 2015, **54**, 10271–10275.
6 M.-A. Légaré, C. Pranckevicius and H. Braunschweig, Metallomimetic Chemistry of Boron, *Chem. Rev.*, 2019, **119**, 8231–8261.
7 J. Poater, S. Escayola, A. Poater, F. Teixidor, H. Ottosson, C. Viñas and M. Solà, Single—Not Double—3D-Aromaticity in an Oxidized *Closo* Icosahedral Dodecaiodo-Dodecaborate Cluster, *J. Am. Chem. Soc.*, 2023, **145**, 22527–22538.
8 G. Hernández-Juárez, J. Barroso, A. Vásquez-Espinal, F. Ortíz-Chi, W. Tiznado, F. Murillo and G. Merino, Breaking the plane: B_5H_5 is a three-dimensional structure, *Phys. Chem. Chem. Phys.*, 2024, **26**, 8089–8093.
9 M. Michel, S. Kar, L. Endres, R. D. Dewhurst, B. Engels and H. Braunschweig, The synthesis of a neutral boryne, *Nat. Synth.*, 2025, **4**, 869–876.
10 J. Barthel, M. Wühr, R. Buestrich and H. J. Gores, A New Class of Electrochemically and Thermally Stable Lithium Salts for Lithium Battery Electrolytes: I. Synthesis and Properties of Lithium bis[1,2-benzenediolato(2−)–O,O′] borate, *J. Electrochem. Soc.*, 1995, **142**, 2527–2531.
11 J. Barthel, R. Buestrich, H. J. Gores, M. Schmidt and M. Wühr, A New Class of Electrochemically and Thermally Stable Lithium Salts for Lithium Battery Electrolytes: IV. Investigations of the Electrochemical Oxidation of Lithium Organoborates, *J. Electrochem. Soc.*, 1997, **144**, 3866–3870.
12 K. Xu, S. Zhang, T. R. Jow, W. Xu and C. A. Angell, LiBOB as Salt for Lithium-Ion Batteries: A Possible Solution for High Temperature Operation, *Electrochem. Solid-State Lett.*, 2002, **5**, A26–A29.
13 M. Ue, T. Fujii, Z.-B. Zhou, M. Takeda and S. Kinoshita, Electrochemical properties of $Li[C_nF_{2n+1}BF_3]$ as electrolyte

salts for lithium-ion cells, *Solid State Ionics*, 2006, **177**, 323–331.
14 S. S. Zhang, An unique lithium salt for the improved electrolyte of Li-ion battery, *Electrochem. Commun.*, 2006, **8**, 1423–1428.
15 J. Scheers, P. Johansson and P. Jacobsson, Anions for Lithium Battery Electrolytes: A Spectroscopic and Theoretical Study of the $B(CN)_4^-$ Anion of the Ionic Liquid $C_2^{mim}[B(CN)_4]$, *J. Electrochem. Soc.*, 2008, **155**, A628–A634.
16 J. Luo, Y. Bi, L. Zhang, X. Zhang and T. L. Liu, A Stable, Non-corrosive Perfluorinated Pinacolatoborate Mg Electrolyte for Rechargeable Mg Batteries, *Angew. Chem.*, 2019, **131**, 7041–7045.
17 Z. Huang, S. Wang, R. D. Dewhurst, N. V. Ignat'ev, M. Finze and H. Braunschweig, Boron: Its Role in Energy-Related Processes and Applications, *Angew. Chem., Int. Ed.*, 2020, **59**, 8800–8816.
18 Q. Wu, M. Esteghamatian, N.-X. Hu, Z. Popovic, G. Enright, Y. Tao, M. D'Iorio and S. Wang, Synthesis, Structure, and Electroluminescence of BR_2q (R = Et, Ph, 2-Naphthyl and q = 8-Hydroxyquinolato), *Chem. Mater.*, 2000, **12**, 79–83.
19 Y.-L. Rao and S. Wang, Four-Coordinate Organoboron Compounds with a π-Conjugated Chelate Ligand for Optoelectronic Applications, *Inorg. Chem.*, 2011, **50**, 12263–12274.
20 D. Li, H. Zhang and Y. Wang, Four-coordinate organoboron compounds for organic light-emitting diodes (OLEDs), *Chem. Soc. Rev.*, 2013, **42**, 8416–8433.
21 H.-B. Cheng, X. Cao, S. Zhang, K. Zhang, Y. Cheng, J. Wang, J. Zhao, L. Zhou, X.-J. Liang and J. Yoon, BODIPY as a Multifunctional Theranostic Reagent in Biomedicine: Self-Assembly, Properties, and Applications, *Adv. Mater.*, 2023, **35**, 2207546.
22 F. Yang, M. Zhu, J. Zhang and H. Zhou, Synthesis of biologically active boron-containing compounds, *Med. Chem. Commun.*, 2018, **9**, 201–211.
23 S. Chatterjee, N. M. Tripathi and A. Bandyopadhyay, The modern role of boron as a 'magic element' in biomedical science: chemistry perspective, *Chem. Commun.*, 2021, **57**, 13629–13640.
24 B. C. Das, M. A. Shareef, S. Das, N. K. Nandwana, Y. Das, M. Saito and L. M. Weiss, Boron-Containing heterocycles as promising pharmacological agents, *Bioorg. Med. Chem.*, 2022, **63**, 116748.
25 H. Braunschweig, T. Dellermann, R. D. Dewhurst, W. C. Ewing, K. Hammond, J. O. C. Jimenez-Halla, T. Kramer, I. Krummenacher, J. Mies, A. K. Phukan and A. Vargas, Metal-free binding and coupling of carbon monoxide at a boron-boron triple bond, *Nat. Chem.*, 2013, **5**, 1025–1028.
26 M. Arrowsmith, J. Böhnke, H. Braunschweig, M. A. Celik, C. Claes, W. C. Ewing, I. Krummenacher, K. Lubitz and C. Schneider, Neutral Diboron Analogues of Archetypal Aromatic Species by Spontaneous Cycloaddition, *Angew. Chem., Int. Ed.*, 2016, **55**, 11271–11275.
27 Y. Su, Y. Li, R. Ganguly and R. Kinjo, Engineering the Frontier Orbitals of a Diazadiborinine for Facile Activation of H_2, NH_3, and an Isonitrile, *Angew. Chem., Int. Ed.*, 2018, **57**, 7846–7849.
28 S. Yruegas, D. C. Patterson and C. D. Martin, Oxygen insertion into boroles as a route to 1,2-oxaborines, *Chem. Commun.*, 2016, **52**, 6658–6661.
29 J. H. Barnard, S. Yruegas, K. Huang and C. D. Martin, Ring expansion reactions of anti-aromatic boroles: a promising synthetic avenue to unsaturated boracycles, *Chem. Commun.*, 2016, **52**, 9985–9991.
30 Y. Su and R. Kinjo, Small molecule activation by boron-containing heterocycles, *Chem. Soc. Rev.*, 2019, **48**, 3613–3659.
31 Z.-F. Zhang and M.-D. Su, Understanding the CO capture reaction through electronic structure analysis of four-membered-ring group-13/N- and B/group-15-based Lewis acid-base pairs, *RSC Adv.*, 2024, **14**, 19446–19458.
32 P. Paetzold, B. Redenz-Stormanns and R. Boese, Boroboration of CO with Tri–*tert*–butylazadiboriridine, *Angew. Chem., Int. Ed. Engl.*, 1990, **29**, 900–902.
33 J. Teichmann, H. Stock, H. Pritzkow and W. Siebert, Carbon Monoxide and Isonitrile Insertion into the B–B Bond of Five-Membered Cyclic Organo-1,2-diboranes, *Eur. J. Inorg. Chem.*, 1998, **1998**, 459–463.
34 A. Fukazawa, J. L. Dutton, C. Fan, L. G. Mercier, A. Y. Houghton, Q. Wu, W. E. Piers and M. Parvez, Reaction of pentaarylboroles with carbon monoxide: an isolable organoboron carbonyl complex, *Chem. Sci.*, 2012, **3**, 1814–1818.
35 W. Haubold and A. Gemmler, Darstellung und Eigenschaften von Diborheterocyclen, *Chem. Ber.*, 1980, **113**, 3352–3356.
36 W. Siebert, H. Schmidt and R. Full, Darstellung und Ligandeneigenschaften eines 1.2.5-Azadiborolen-Derivates [1]/Synthesis and Ligand Properties of an 1,2,5-Azadiborolene Derivative [1], *Z. Naturforsch., B*, 1980, **35**, 873–881.
37 P. Paetzold, B. Redenz-Stormanns and R. Boese, Reaktionen der Azadiboriridine: Clusterbildung und Ringerweiterung, *Chem. Ber.*, 1991, **124**, 2435–2441.
38 R. Köster, G. Seidel and R. Boese, Ethyl-substituierte 2,5-Dihydro-1,2,5-oxadiborole, *Chem. Ber.*, 1994, **127**, 2159–2165.
39 S. Luckert, E. Eversheim, U. Englert, T. Wagner and P. Paetzold, Reactions at the B-B Bond of Tri-*tert*-butylazadiboriridine NB_2R_3: Ring Extensions, *Z. Anorg. Allg. Chem.*, 2001, **627**, 1815–1823.
40 W. K. Brown, K. K. Klausmeyer and B. M. Lindley, Unlocking metal coordination of diborylamides through ring constraints, *Chem. Commun.*, 2022, **58**, 867–870.
41 C. Hu, L. Guo, J. Zhang and C. Cui, C–C Activation to BNB-Embedded Indenophenanthrenes. Electronic Structure and Reactivity, *Organometallics*, 2021, **40**, 1015–1019.
42 H. Wei, Y. Liu, T. Y. Gopalakrishna, H. Phan, X. Huang, L. Bao, J. Guo, J. Zhou, S. Luo, J. Wu and Z. Zeng, B–N–B

Bond Embedded Phenalenyl and Its Anions, *J. Am. Chem. Soc.*, 2017, **139**, 15760–15767.

43 X.-Y. Wang, A. Narita, X. Feng and K. Müllen, B_2N_2-Dibenzo[*a*,*e*]pentalenes: Effect of the BN Orientation Pattern on Antiaromaticity and Optoelectronic Properties, *J. Am. Chem. Soc.*, 2015, **137**, 7668–7671.

44 M. J. Frisch, G. W. Trucks, H. B. Schlegel, G. E. Scuseria, M. A. Robb, J. R. Cheeseman, G. Scalmani, V. Barone, B. Mennucci, G. A. Petersson, H. Nakatsuji, M. Caricato, X. Li, H. P. Hratchian, A. F. Izmaylov, J. Bloino, G. Zheng, J. L. Sonnenberg, M. Hada, M. Ehara, K. Toyota, R. Fukuda, J. Hasegawa, M. Ishida, T. Nakajima, Y. Honda, O. Kitao, H. Nakai, T. Vreven, J. A. Montgomery, J. E. Peralta, F. Ogliaro, M. Bearpark, J. J. Heyd, E. Brothers, K. N. Kudin, V. N. Staroverov, T. Keith, R. Kobayashi, J. Normand, K. Raghavachari, A. Rendell, J. C. Burant, S. S. Iyengar, J. Tomasi, M. Cossi, N. Rega, J. M. Millam, M. Klene, J. E. Knox, J. B. Cross, V. Bakken, C. Adamo, J. Jaramillo, R. Gomperts, R. E. Stratmann, O. Yazyev, A. J. Austin, R. Cammi, C. Pomelli, J. W. Ochterski, R. L. Martin, K. Morokuma, V. G. Zakrzewski, G. A. Voth, P. Salvador, J. J. Dannenberg, S. Dapprich, A. D. Daniels, O. Farkas, J. B. Foresman, J. V. Ortiz, J. Cioslowski and D. J. Fox, *Gaussian 09, Revision D. 01*, Gaussian, Inc., Wallingford CT, 2013.

45 J.-D. Chai and M. Head-Gordon, Long-range corrected hybrid density functionals with damped atom-atom dispersion corrections, *Phys. Chem. Chem. Phys.*, 2008, **10**, 6615–6620.

46 F. Weigend and R. Ahlrichs, Balanced basis sets of split valence, triple zeta valence and quadruple zeta valence quality for H to Rn: Design and assessment of accuracy, *Phys. Chem. Chem. Phys.*, 2005, **7**, 3297–3305.

47 A. V. Marenich, C. J. Cramer and D. G. Truhlar, Universal Solvation Model Based on Solute Electron Density and on a Continuum Model of the Solvent Defined by the Bulk Dielectric Constant and Atomic Surface Tensions, *J. Phys. Chem. B*, 2009, **113**, 6378–6396.

48 L. Goerigk and S. Grimme, A thorough benchmark of density functional methods for general main group thermochemistry, kinetics, and noncovalent interactions, *Phys. Chem. Chem. Phys.*, 2011, **13**, 6670–6688.

49 M. Bursch, J.-M. Mewes, A. Hansen and S. Grimme, Best-Practice DFT Protocols for Basic Molecular Computational Chemistry, *Angew. Chem., Int. Ed.*, 2022, **61**, e202205735, (*Angew. Chem.*, 2022, **134**, e202205735).

50 R. G. Parr, L. v. Szentpály and S. Liu, Electrophilicity Index, *J. Am. Chem. Soc.*, 1999, **121**, 1922–1924.

51 R. G. Pearson, Absolute electronegativity and hardness: application to inorganic chemistry, *Inorg. Chem.*, 1988, **27**, 734–740.

52 T. Koopmans, Über die Zuordnung von Wellenfunktionen und Eigenwerten zu den Einzelnen Elektronen Eines Atoms, *Physica*, 1934, **1**, 104–113.

53 P. K. Chattaraj and D. R. Roy, Update 1 of: Electrophilicity Index, *Chem. Rev.*, 2007, **107**, PR46–PR74.

54 A. R. Jupp, T. C. Johnstone and D. W. Stephan, The global electrophilicity index as a metric for Lewis acidity, *Dalton Trans.*, 2018, **47**, 7029–7035.

55 R. Pal and P. K. Chattaraj, Electrophilicity index revisited, *J. Comput. Chem.*, 2023, **44**, 278–297.

56 D. I. Martínez-Valencia, L. I. Lugo-Fuentes, G. González-García, J. A. Luján-Montelongo, K. J. Shea, J. E. Báez and J. O. C. Jiménez-Halla, Computational study of polyhomologation: understanding reactivity with B, Al, and Ga, *New J. Chem.*, 2025, **49**, 6936–6945.

57 T. Lu, Simple, reliable, and universal metrics of molecular planarity, *J. Mol. Model.*, 2021, **27**, 263.

58 A. Poater, F. Ragone, S. Giudice, C. Costabile, R. Dorta, S. P. Nolan and L. Cavallo, Thermodynamics of N-Heterocyclic Carbene Dimerization: The Balance of Sterics and Electronics, *Organometallics*, 2008, **27**, 2679–2681.

59 A. Poater, B. Cosenza, A. Correa, S. Giudice, F. Ragone, V. Scarano and L. Cavallo, Samb*V*ca: A Web Application for the Calculation of the Buried Volume of N-Heterocyclic Carbene Ligands, *Eur. J. Inorg. Chem.*, 2009, **2009**, 1759–1766.

60 L. Falivene, Z. Cao, A. Petta, L. Serra, A. Poater, R. Oliva, V. Scarano and L. Cavallo, Towards the online computer-aided design of catalytic pockets, *Nat. Chem.*, 2019, **11**, 872–879.

61 S. Escayola, N. Bahri-Laleh and A. Poater, $\%V_{Bur}$ index and steric maps: from predictive catalysis to machine learning, *Chem. Soc. Rev.*, 2024, **53**, 853–882.

62 E. D. Glendenning, A. E. Reed, J. E. Carpenter and F. Weinhold, *NBO Version 3.1*, 2001.

63 T. Lu and F. Chen, Multiwfn: A multifunctional wavefunction analyzer, *J. Comput. Chem.*, 2012, **33**, 580–592.

64 I. Mayer, Charge, bond order and valence in the AB initio SCF theory, *Chem. Phys. Lett.*, 1983, **97**, 270–274.

65 K. B. Wiberg, Application of the pople-santry-segal CNDO method to the cyclopropylcarbinyl and cyclobutyl cation and to bicyclobutane, *Tetrahedron*, 1968, **24**, 1083–1096.

66 O. V. Sizova, L. V. Skripnikov and A. Y. Sokolov, Symmetry decomposition of quantum chemical bond orders, *J. Mol. Struct.: THEOCHEM*, 2008, **870**, 1–9.

67 M. Giambiagi, M. S. de Giambiagi and K. C. Mundim, Definition of a multicenter bond index, *Struct. Chem.*, 1990, **1**, 423–427.

68 P. Bultinck, R. Ponec and S. Van Damme, Multicenter bond indices as a new measure of aromaticity in polycyclic aromatic hydrocarbons, *J. Phys. Org. Chem.*, 2005, **18**, 706–718.

69 E. Matito, An electronic aromaticity index for large rings, *Phys. Chem. Chem. Phys.*, 2016, **18**, 11839–11846.

70 T. Lu, A comprehensive electron wavefunction analysis toolbox for chemists, Multiwfn, *J. Chem. Phys.*, 2024, **161**, 082503.

71 D. Rappoport and F. Furche, Property-optimized Gaussian basis sets for molecular response calculations, *J. Chem. Phys.*, 2010, **133**, 134105.

72 Z. Wang, Y. Zhou, T. B. Marder and Z. Lin, DFT studies on reactions of boroles with carbon monoxide, *Org. Biomol. Chem.*, 2017, **15**, 7019–7027.
73 M. J. D. Bosdet and W. E. Piers, B-N as a C-C substitute in aromatic systems, *Can. J. Chem.*, 2009, **87**, 8–29.
74 X. Wang, G. Sun, P. Routh, D.-H. Kim, W. Huang and P. Chen, Heteroatom-doped graphene materials: syntheses, properties and applications, *Chem. Soc. Rev.*, 2014, **43**, 7067–7098.
75 X.-Y. Wang, J.-Y. Wang and J. Pei, BN Heterosuperbenzenes: Synthesis and Properties, *Chem. – Eur. J.*, 2015, **21**, 3528–3539.
76 P. B. Pati, E. Jin, Y. Kim, Y. Kim, J. Mun, S. J. Kim, S. J. Kang, W. Choe, G. Lee, H.-J. Shin and Y. S. Park, Unveiling 79-Year-Old Ixene and Its BN-Doped Derivative, *Angew. Chem., Int. Ed.*, 2020, **59**, 14891–14895.
77 M. Chen, K. S. Unikela, R. Ramalakshmi, B. Li, C. Darrigan, A. Chrostowska and S.-Y. Liu, A BN–Doped Cycloparaphenylene Debuts, *Angew. Chem., Int. Ed.*, 2021, **60**, 1556–1560.
78 X. Chen, D. Tan and D.-T. Yang, Multiple-boron–nitrogen (multi-BN) doped π-conjugated systems for optoelectronics, *J. Mater. Chem. C*, 2022, **10**, 13499–13532.
79 F. Feixas, E. Matito, M. Solà and J. Poater, Analysis of Hückel's [4n + 2] Rule through Electronic Delocalization Measures, *J. Phys. Chem. A*, 2008, **112**, 13231–13238.
80 F. Feixas, E. Matito, M. Solà and J. Poater, Patterns of π-electron delocalization in aromatic and antiaromatic organic compounds in the light of Hückel's 4n + 2 rule, *Phys. Chem. Chem. Phys.*, 2010, **12**, 7126–7137.
81 F. Feixas, E. Matito, J. Poater and M. Solà, Quantifying aromaticity with electron delocalisation measures, *Chem. Soc. Rev.*, 2015, **44**, 6434–6451.
82 N. C. Baird, Quantum Organic Photochemistry. II. Resonance and Aromaticity in the Lowest $^3\pi\pi^*$ State of Cyclic Hydrocarbons, *J. Am. Chem. Soc.*, 1972, **94**, 4941–4948.
83 A. Soncini and P. W. Fowler, Ring-current aromaticity in open-shell systems, *Chem. Phys. Lett.*, 2008, **450**, 431–436.
84 F. Feixas, J. Vandenbussche, P. Bultinck, E. Matito and M. Solà, Electron delocalization and aromaticity in low-lying excited states of archetypal organic compounds, *Phys. Chem. Chem. Phys.*, 2011, **13**, 20690–20703.
85 P. R. von Schleyer and H. Jiao, What is aromaticity?, *Pure Appl. Chem.*, 1996, **68**, 209–218.
86 V. I. Minkin, Glossary of terms used in theoretical organic chemistry, *Pure Appl. Chem.*, 1999, **71**, 1919–1981.
87 R. Boese, A. H. Maulitz and P. Stellberg, Solid-State Borazine: Does it Deserve to be Entitled "Inorganic Benzene"?, *Chem. Ber.*, 1994, **127**, 1887–1889.
88 M. del R. Merino-García, L. A. Soriano-Agueda, J. de D. Guzmán-Hernández, D. Martínez-Otero, B. L. Rivera, F. Cortés-Guzmán, J. E. Barquera-Lozada and V. Jancik, Benzene and Borazine, so Different, yet so Similar: Insight from Experimental Charge Density Analysis, *Inorg. Chem.*, 2022, **61**, 6785–6798.
89 M. Yáñez, O. Mó, I. Alkorta and J. E. Del Bene, Structures, Bonding, and One-Bond B–N and B–H Spin–Spin Coupling Constants for a Series of Neutral and Anionic Five-Membered Rings Containing BN Bonds, *J. Chem. Theory Comput.*, 2008, **4**, 1869–1876.
90 R. Hoffmann, Building Bridges Between Inorganic and Organic Chemistry (Nobel Lecture), *Angew. Chem., Int. Ed. Engl.*, 1982, **21**, 711–724.
91 C. G. Wermuth, C. R. Ganellin, P. Lindberg and L. A. Mitscher, Glossary of terms used in medicinal chemistry (IUPAC Recommendations 1998), *Pure Appl. Chem.*, 1998, **70**, 1129–1143.
92 I. Ghesner, W. E. Piers, M. Parvez and R. McDonald, Lewis Acid Chelation of $[NR]^{2-}$ by 2,2′-Diborabiphenyl: 9,11-Diboratacarbazole Heterocycles, *Organometallics*, 2004, **23**, 3085–3087.
93 C. Li, D. Xie, Z. Ye, Z. Zhang and F. Wang, Boron-containing organic electroluminescent compound and application thereof on organic electroluminescent devices, *CN Pat*, 111471064A, 2020.
94 T. Bischof, L. Beßler, I. Krummenacher, L. Erhard, H. Braunschweig and M. Finze, Construction of a Diverse Range of Boron Heterocycles via Ring Expansion of a Carboranyl-Substituted 9-Borafluorene, *Chem. – Eur. J.*, 2023, **29**, e202300210.
95 Following recommendations by Grimme and coworkers (ref. 49), a representative recalculation of barrier heights regarding the ring expansion reaction of **1** (Fig. 1) and **8** (Table 1/Fig. 4) was conducted applying the higher quality DFT method ωB97X-D/def2-TZVPP. The energy barrier increased by 0.1 (**1**) and decreased by 0.9 kcal mol^{-1} (**8**) in comparison with previously discussed values at the ωB97X-D/def2-TZVPP//ωB97X-D/def2-SVP level. Hence, the principal computational method employed herein ensures that the basis-set errors are negligible concerning the established thermochemistry data. The Cartesian coordinates of the reoptimized geometries are reported in Table S12.

